

Article

Coverage and Spectral Efficiency of Network Assisted Full Duplex in a Millimeter Wave System

Yingli He ¹, Dongqin Zhao ^{2,*}, Zhenqi Fan ¹, An Lu ¹, Xinjiang Xia ^{2,3,*} and Dongming Wang ²

¹ State Grid Electric Power Research Institute, Nanjing 211100, China; heyngli@sgepri.sgcc.com.cn (Y.H.); fanzhenqi1@sgepri.sgcc.com.cn (Z.F.); luan@sgepri.sgcc.com.cn (A.L.)

² National Mobile Communications Research Laboratory, Southeast University, Nanjing 210096, China; wangdm@seu.edu.cn

³ Purple Mountain Laboratories, Nanjing 211111, China

* Correspondence: 220190948@seu.edu.cn (D.Z.); xinjiang_xia@seu.edu.cn (X.X.)

Abstract: To cope with the growing trend of asymmetric data traffic, we introduce a novel network assisted full duplex (NAFD) for a millimeter wave system. NAFD can dynamically allocate the number of remote radio heads in the uplink mode or in the downlink mode, which can facilitate simultaneous uplink and downlink communications. In this manuscript, we use stochastic geometry to analyze the distribution of the signal-to-interference-plus-noise ratio and the data rate in a NAFD system. The numerical results verify the analysis and show that the NAFD outperforms the dynamic time division duplex system and the traditional flexible duplex system in terms of spectral efficiency.

Keywords: network assisted full duplex; stochastic geometry; SINR; spectral efficiency



Citation: He, Y.; Zhao, D.; Fan, Z.; Lu, A.; Wang, D. Coverage and Spectral Efficiency of Network Assisted Full Duplex in a Millimeter Wave System. *Electronics* **2022**, *11*, 5. <https://doi.org/10.3390/electronics11010005>

Academic Editor: Raed A. Abd-Alhameed

Received: 12 November 2021

Accepted: 15 December 2021

Published: 21 December 2021

Publisher's Note: MDPI stays neutral with regard to jurisdictional claims in published maps and institutional affiliations.



Copyright: © 2021 by the authors. Licensee MDPI, Basel, Switzerland. This article is an open access article distributed under the terms and conditions of the Creative Commons Attribution (CC BY) license (<https://creativecommons.org/licenses/by/4.0/>).

1. Introduction

Network densification by using small cells in fifth generation cellular communication systems (5G) could increase the traffic load between different cells significantly [1,2]. In addition, as the popularization of various wireless smart devices and the surge of the user's mobility, the traffic asymmetry between the uplink and downlink will continue to increase [3,4]. Therefore, future communication systems need more flexible technologies to cope with the situation of huge traffic volumes and asymmetric uplink and downlink services.

Traditional frequency division duplex (FDD) systems usually employ the paired frequency bands for uplink and downlink transmissions [5], which is difficult to meet the demand of asymmetric data services. Asymmetric FDD carrier aggregation can solve the problem, whereas leads to increased cost and power consumption [6,7]. In contrast, time division duplex (TDD) systems do not require paired frequencies. It can use an asymmetric time slot configuration in the uplink and downlink according to the actual situation [8,9]. Due to the asymmetry of spatio-temporal traffic, the synchronization slot configuration is extremely inefficient for small cellular networks. Xin et al. [10] proposed a method of adjusting the number of base stations in the uplink or the downlink modes in a flexible manner to solve the traffic asymmetry problem. In the system proposed by Xin et al., each base station can flexibly adjust its working state (uplink or downlink) without strict synchronization with other base stations; thus, reducing the overhead of the synchronization signal.

Recently, a unified duplex technique called network assisted full duplex (NAFD) has been presented to combine flexible duplex, hybrid-duplex, full duplex and other duplex methods by using cell-free massive MIMO network method [11]. By taking advantage of the virtue of joint processing, such as the downlink-to-uplink interference cancellation in the digital domain and genetic algorithm based user scheduling, cross-link interference has been alleviated to a large extent. NAFD technique could fully exploit the spatial degree-of-freedom of distributed networks and triggers further research interests. Millimeter wave (mmWave) propagation is a key enabling technique for 5G system. In mmWave

band, phased array technique could be used to reduce implementation complexity of the transceiver. With narrow beam, spatial domain duplex could be possible. In this paper, we introduce NAFD to mmWave system with phased array. For mmWave systems, we can use narrow beams to reduce the cross-link interference which is the main challenge for sub-6GHz systems with NAFD.

In [11], the spectral efficiency analysis have been given by using random matrix theory. However, the system-level performance of NAFD has not been studied. Stochastic geometry is a useful tool for analyzing the performance of traditional cellular network systems [12,13]. The total signal-to-interference-plus-noise ratio (SINR) coverage probability was derived in a simple form by modeling the location of the base station in a traditional cellular network as a poisson point process (PPP) on a two-dimensional Euclidean plane [14]. In addition, it has been verified that the SINR coverage probability derived from the stochastic geometry tool is the lower bound of the SINR coverage probability derived from the actual cellular network location deployment [14,15]. The application of stochastic geometry is not limited to conventional cellular networks but also mmWave cellular networks. A general framework was proposed to evaluate the coverage and rate performance in mmWave cellular networks that leverages concepts from stochastic geometry [16].

This study analyzes the SINR coverage probability and spectral efficiency of a mmWave system with NAFD based on a stochastic geometry framework. The results show that the NAFD outperforms the dynamic TDD system and the traditional flexible duplex system in spectral efficiency.

The remainder of this paper is organized as follows. Section 2 introduces the NAFD system model, which includes the concept of NAFD, the remote radio head (RRH) and user location deployment, directional antenna models, and channel fading. Section 3 mathematically derives the distribution of the downlink and uplink SINR based on the conclusions of stochastic geometry. Section 4 mathematically derives the coverage probability of the instantaneous achievable rate and the average achievable rate. Section 5 provides the numerical results and discussions. Finally, Section 6 concludes this paper.

2. System Model

2.1. Concept of NAFD for mmWave System

In this paper, we consider a mmWave system with NAFD, which is composed of a baseband unit (BBU) and several RRHs. The RRHs are connected to the BBU through a high-speed optical cable, and multiple BBUs are grouped together for real-time signal processing by the cloud computing platform. The RRH could be with half-duplex or full-duplex. To reduce the hardware implementation, we consider half-duplex RRH. In NAFD systems, both uplink and downlink transmission use the same resource blocks, and the BBU determines whether the RRH works in the uplink mode or the downlink mode [11]. Cross-link interferences, including downlink-to-uplink and uplink-to-downlink interferences will be a main challenge in NAFD. Since all the RRHs are connected to the BBU, downlink-to-uplink interference can be cancelled in digital domain. The spectral efficiency of NAFD could be better than that of dynamic TDD with downlink-to-uplink interference cancellation [11].

2.2. RRH and User Deployment

This study assumed that the RRHs are located according to a homogeneous PPP of density λ_R in the Euclidean plane. The probabilities of RRH in the downlink mode and the uplink mode are denoted by p_D and p_U respectively, where $p_D + p_U = 1$. By the thinning theorem of the PPP [12,13], the locations of the RRHs in the downlink mode and the uplink mode can be modeled as two independent homogeneous PPPs Φ_R^D and Φ_R^U with densities $p_D\lambda_R$ and $p_U\lambda_R$, respectively.

Before associating with a particular RRH, the mobile user locations follow a homogeneous PPP with density λ_U . It is assumed that each user is associated with the nearest base station; hence, the users of each RRH are uniformly distributed in the Voronoi cell

of the RRH [17]. It is also assumed that each RRH serves a single active user on a given time-frequency resource, which is randomly selected from all users in its Voronoi cell. Figure 1 shows a schematic diagram of the RRH and user deployment of the NAFD system when $\lambda_R = 10^{-3}$ RRH/m² and $p_D = p_U = 1/2$.

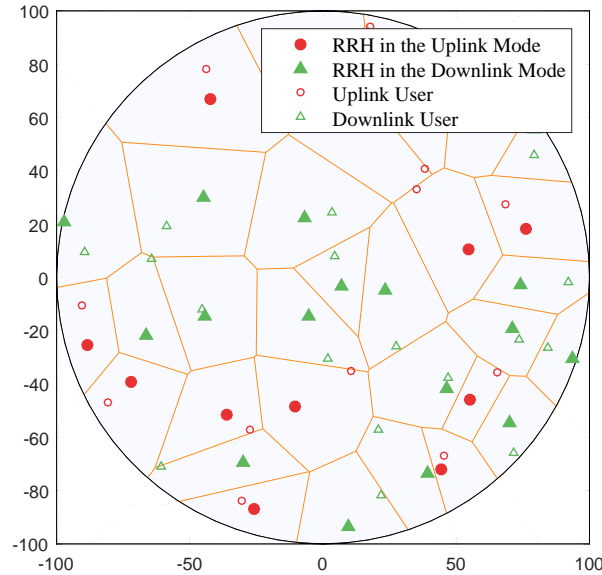


Figure 1. A diagram of the RRH and user deployment of the NAFD system.

2.3. Directional Beamforming

In this paper, both RRHs and user terminals use phased array technique to perform directional beamforming. For tractability of the analysis, a sectored antenna model is exploited to approximate the array patterns [16] and perfect beam alignment is also adopted. Let $G_{M,m,\theta}(\phi)$ denote the sector antenna model in Figure 2, where M is the main lobe directivity gain, m is the back lobe gain, θ is the beamwidth of the main lobe, and ϕ is the angle off the boresight direction. The antenna gain is assumed to be constant M when the angle ϕ is in the main lobe and constant m when the angle ϕ is in the back lobe. Without loss of generality, the antenna’s boresight direction is assumed to be 0° , then:

$$G_{M,m,\theta}(\phi) = \begin{cases} M, & \phi \leq |\theta/2|, \\ m, & \phi \geq |\theta/2|. \end{cases} \quad (1)$$

Let M_R , m_R , and θ_R be the main lobe gain, side lobe gain, and half beamwidth of the RRH antenna, respectively. In addition, M_U , m_U , and θ_U are the corresponding parameters of the user’s antenna.

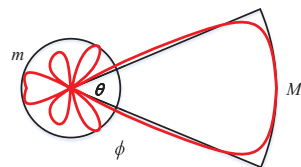


Figure 2. A sectored model to approximate the beamforming patterns.

In the downlink, the total antenna gain from the i -th RRH in the downlink mode to the typical downlink user can be denoted by $A_i = G_{M_R,m_R,\theta_R}(\phi_R^i)G_{M_U,m_U,\theta_U}(\phi_U^i)$, where ϕ_R^i and ϕ_U^i indicate the angle of departure and the angle of arrival, respectively. Since the typical downlink user is associated with the nearest RRH, both the typical user and its serving RRH will estimate the downlink channel. This includes the angle of arrival and fading, and then it adjusts the antenna steering direction accordingly to exploit the

maximum directional gain. This study ignored the error in the channel estimation and the synchronization error of the time and carrier frequency. Therefore, the directional gain for the desired downlink is $M_R M_U$. For the i -th interfering link, the angles ϕ_R^i and ϕ_U^i are assumed to be independently and uniformly distributed in $(0, 2\pi]$. As a result, the directional gain A_i is a discrete random variable with the probability distribution as $A_i = a_k^1$ with the probability b_k^1 . The probability mass function of A_i is shown in Table 1.

Table 1. Probability mass function of A_i .

k	1	2	3	4
a_k^1	$M_R M_U$	$M_R m_U$	$m_R M_U$	$m_R m_U$
b_k^1	$\frac{\theta_R \theta_U}{4\pi^2}$	$\frac{\theta_R (2\pi - \theta_U)}{4\pi^2}$	$\frac{(2\pi - \theta_R) \theta_U}{4\pi^2}$	$\frac{(2\pi - \theta_R)(2\pi - \theta_U)}{4\pi^2}$

Let $B_i = G_{M_{U_1}, m_{U_1}, \theta_{U_1}}(\phi_{U_1}^i) G_{M_{U_2}, m_{U_2}, \theta_{U_2}}(\phi_{U_2}^i)$ denote the total antenna gain from the i -th interfering uplink user to the typical downlink user, where $\phi_{U_1}^i$ and $\phi_{U_2}^i$ indicate the angle of departure and the angle of arrival, respectively. The angles $\phi_{U_1}^i$ and $\phi_{U_2}^i$ are assumed to be independently and uniformly distributed in $(0, 2\pi]$. As a result, the directional gain B_i is a discrete random variable with the probability distribution as $B_i = a_k^2$ with the probability b_k^2 . The probability mass function of B_i is shown in Table 2.

Table 2. Probability mass function of B_i .

k	1	2	3
a_k^2	M_U^2	$M_U m_U$	m_U^2
b_k^2	$\frac{\theta_U^2}{4\pi^2}$	$\frac{\theta_U (2\pi - \theta_U)}{2\pi^2}$	$\frac{(2\pi - \theta_U)^2}{4\pi^2}$

In the uplink, let $C_i = G_{M_U, m_U, \theta_U}(\phi_U^i) G_{M_R, m_R, \theta_R}(\phi_R^i)$ denote the total antenna gain from the i -th typical uplink user to the tagged RRH, which is in the uplink mode and is the serving RRH of the typical uplink user, where ϕ_U^i and ϕ_R^i indicate the angle of departure and the angle of arrival, respectively. Similar to the downlink transmission, the directional gain for the desired uplink is $M_U M_R$. For the i -th interfering link, the angles ϕ_U^i and ϕ_R^i are assumed to be independently and uniformly distributed in $(0, 2\pi]$. Therefore, the discrete random variable C_i has the same probability mass function as A_i .

Let $D_i = G_{M_{R_1}, m_{R_1}, \theta_{R_1}}(\phi_{R_1}^i) G_{M_{R_2}, m_{R_2}, \theta_{R_2}}(\phi_{R_2}^i)$ denote the total antenna gain from the i -th interfering RRH in the downlink mode to the tagged RRH in the uplink mode, where $\phi_{R_1}^i$ and $\phi_{R_2}^i$ indicate the angle of departure and the angle of arrival, respectively. The angles $\phi_{R_1}^i$ and $\phi_{R_2}^i$ are assumed to be independently and uniformly distributed in $(0, 2\pi]$. As a result, the directional gain D_i is a discrete random variable with the probability distribution as $D_i = a_k^3$ with the probability b_k^3 . The probability mass function of D_i is shown in Table 3.

Table 3. Probability mass function of D_i .

k	1	2	3
a_k^3	M_R^2	$M_R m_R$	m_R^2
b_k^3	$\frac{\theta_R^2}{4\pi^2}$	$\frac{\theta_R (2\pi - \theta_R)}{2\pi^2}$	$\frac{(2\pi - \theta_R)^2}{4\pi^2}$

2.4. Channel Fading and Power Allocation

Channel fading includes large-scale fading and small-scale fading. Regarding large-scale fading, assuming that the path loss model is $PL(d) = Kd^{-\alpha}$, where α ($\alpha > 2$) represents the path loss exponents, while K represents the path loss at the reference distance $d = 1$. It is assumed that the small-scale fading is modeled as Rayleigh fading; hence, the channel power gain is subject to exponential distribution. Without loss of generality,

supposing that the mean of the exponential distribution is 1. This study used $g, h, g',$ and h' to denote the channel power gain of the RRH-to-user link, user-to-user link, RRH-to-RRH link, and user-to-RRH link, respectively. As a result, $g, h, g',$ and h' are independent and identically distributed (i.i.d) random variables.

In the downlink, the RRH transmission powers are assumed to be a constant P_R . In the uplink, mobile users use distance-proportional fractional power control [14]. For example, the transmission power of the uplink user is $P_U K^{-\epsilon} R^{\epsilon\alpha}$, where R is the distance from the uplink user to its serving RRH, and $\epsilon \in [0, 1]$ is the power control factor. This includes the special case of fixed transmission power ($\epsilon = 0$) and perfect channel inversion ($\epsilon = 1$). In the case of power control, as the user approaches the desired RRH, the transmission power required to maintain the same received signal power is reduced.

3. SINR Coverage Analysis

The SINR coverage probability $P_S(y)$ is defined as the probability that the received SINR is larger than some threshold y ($y > 0$), i.e., the complementary cumulative distribution function (CCDF) of SINR:

$$P_S(y) = \mathbb{P}(\text{SINR} > y). \tag{2}$$

In this sections, we firstly consider the performance of traditional flexible duplex, and then study the performance of NAFD.

3.1. Downlink SINR Coverage Analysis

For downlink transmission, we do not consider the interference cancellation at user terminal side, and we also do not perform the scheduling [11] or user selection [18] to alleviate the uplink-to-downlink interference. Then, in this case, the downlink performance of NAFD is the same as traditional flexible duplex. Without loss of generality, all analysis is for a typical user at the origin, which is denoted by X . It is assumed that the typical user is associated to the nearest RRH, which is in the downlink mode and is denoted by Y_0 . Therefore, the downlink SINR for the typical user can be expressed as:

$$\text{SINR}_{\text{DL}} = \frac{P_R M_R M_U g_{X,Y_0} K D_{X,Y_0}^{-\alpha}}{N_0 + I_D + I_U}, \tag{3}$$

where N_0 is the noise power at the typical user. g_{X,Y_0} denotes the channel power gain from Y_0 to the typical user, and $g_{X,Y_0} \sim \exp(1)$. D_{X,Y_0} is the distance between Y_0 and the typical user. Note that $D_{x,y}$ denotes the distance between the nodes at x and y . I_D denotes the interference received at the typical user from all of the other RRHs in the downlink mode except Y_0 , which can be defined as:

$$I_D = \sum_{Y_i \in \Phi_R^D \setminus \{Y_0\}} A_i P_R g_i K D_{X,Y_i}^{-\alpha}, \tag{4}$$

where g_i denotes the channel power gain from the i -th interfering RRH in the downlink mode to the typical user and $g_i \sim \exp(1)$. A_i denotes the effective antenna gain. I_U denotes the interference received at the typical user from all of the uplink users, which can be defined as:

$$I_U = \sum_{Z_i \in \{\Phi_R^U\}} B_i P_U K^{-\epsilon} D_{Z_i,N(Z_i)}^{\epsilon\alpha} h_i K D_{X,N(Z_i)}^{-\alpha}, \tag{5}$$

where h_i denotes the channel power gain from the i -th interfering uplink user to the typical user, and $h_i \sim \exp(1)$. Z_i denotes the i -th RRH in the uplink mode, and its associated user is $N(Z_i)$. B_i denotes the effective antenna gain.

For convenience and tractability, it is assumed that the distance between the interfering uplink user at $N(Z_i)$ and the typical user at the origin can be approximated to the distance between the RRH at Z_i and the typical user at the origin:

$$D_{X,N(Z_i)} = D_{X,Z_i}. \tag{6}$$

Section 5 will verify the accuracy of the distance approximation in (6). Hence, the interference received at the typical user from all of the uplink users can be approximated to:

$$\hat{I}_U = \sum_{Z_i \in \{\Phi_R^U\}} B_i P_U K^{-\epsilon} D_{Z_i,N(Z_i)}^{\epsilon\alpha} h_i K D_{X,Z_i}^{-\alpha}. \tag{7}$$

Theorem 1. For the flexible duplex system and the NAFD system, the downlink SINR coverage probability can be computed as:

$$P_{S,DL}(y) = \int_0^\infty e^{-s_1 N_0} \mathcal{L}_{I_D}(s_1) \mathcal{L}_{\hat{I}_U}(s_1) f_D(r) dr, \tag{8}$$

where:

$$s_1 = yr^\alpha (P_R M_R M_U K)^{-1}, \tag{9}$$

$$\mathcal{L}_{I_D}(s_1) = \prod_{k=1}^4 \exp \left\{ \frac{2\pi p_D \lambda_R \beta_k^1 r^2 b_k^1}{\alpha - 2} {}_2F_1 \left(1, 1 - \frac{2}{\alpha}; 2 - \frac{2}{\alpha}; \beta_k^1 \right) \right\}, \tag{10}$$

$$\beta_k^1 = -s_1 a_k^1 P_R K r^{-\alpha}, \tag{11}$$

$$\mathcal{L}_{\hat{I}_U}(s_1) = \prod_{k=1}^3 \exp \left\{ -2\pi p_U \lambda_R b_k^2 \mathbb{E}_{D_{Z_i,N(Z_i)}} \left[\int_r^\infty \frac{x dx}{1 + (s_1 a_k^2 P_U K^{-\epsilon} D_{Z_i,N(Z_i)}^{\epsilon\alpha} K)^{-1} x^\alpha} \right] \right\}, \tag{12}$$

$$f_D(r) = 2\pi \lambda_R r e^{-\pi \lambda_R r^2}. \tag{13}$$

Proof of Theorem 1. By using (2), (3), and (7), the probability of the downlink coverage relative to the SINR threshold y can be written as:

$$\begin{aligned} P_{S,DL}(y) &= \mathbb{E}_{D_{X,Y_0}} [\mathbb{P}(\text{SINR}_{DL} > y | D_{X,Y_0})] \\ &= \int_0^\infty \mathbb{P} \left[\frac{P_R M_R M_U g_{X,Y_0} K D_{X,Y_0}^{-\alpha}}{N_0 + I_D + \hat{I}_U} > y | D_{X,Y_0} = r \right] f_D(r) dr \\ &= \int_0^\infty \mathbb{P} [g_{X,Y_0} > yr^\alpha (P_R M_R M_U K)^{-1} (N_0 + I_D + \hat{I}_U)] f_D(r) dr. \end{aligned} \tag{14}$$

Because the locations of the RRHs follow a homogeneous PPP with density λ_R and the users are associated to the nearest RRH [14], the probability density function of D_{X,Y_0} can be found as (13). Let $s_1 = yr^\alpha (P_R M_R M_U K)^{-1}$, and using the fact that $g_{X,Y_0} \sim \exp(1)$, the inner probability term in (14) can be expressed as:

$$\mathbb{P} [g_{X,Y_0} > yr^\alpha (P_R M_R M_U K)^{-1} (N_0 + I_D + \hat{I}_U)] = \mathbb{P} [g_{X,Y_0} > s_1 (N_0 + I_D + \hat{I}_U)] = e^{-s_1 N_0} \mathcal{L}_{I_D + \hat{I}_U}(s_1), \tag{15}$$

where $\mathcal{L}_{I_D + \hat{I}_U}(\cdot)$ is the Laplace transform of the total interference. Since Φ_R^U and Φ_R^D are independent PPPs, $\mathcal{L}_{I_D + \hat{I}_U}(s_1)$ can be rewritten as :

$$\mathcal{L}_{I_D + \hat{I}_U}(s_1) = \mathcal{L}_{I_D}(s_1) \times \mathcal{L}_{\hat{I}_U}(s_1). \tag{16}$$

First, calculate the $\mathcal{L}_{I_D}(s_1)$,

$$\begin{aligned}
 \mathcal{L}_{I_D}(s_1) &= \mathbb{E}\left[e^{-s_1 I_D}\right] = \mathbb{E}_{\Phi_R^D, g_i, A_i} \left[\exp\left(-s_1 \sum_{Y_i \in \Phi_R^D \setminus \{Y_0\}} A_i P_R g_i K D_{X, Y_i}^{-\alpha}\right)\right] \\
 &= \mathbb{E}_{\Phi_R^D} \left\{ \prod_{Y_i \in \Phi_R^D \setminus \{Y_0\}} \mathbb{E}_{g_i, A_i} \left[\exp\left(-s_1 A_i P_R g_i K D_{X, Y_i}^{-\alpha}\right)\right] \right\} \\
 &\stackrel{(a)}{=} \exp\left\{-2\pi p_D \lambda_R \int_r^\infty \left(1 - \mathbb{E}_{g_i, A_i} \left[\exp\left(-s_1 A_i P_R g_i K x^{-\alpha}\right)\right]\right) x dx\right\} \\
 &\stackrel{(b)}{=} \exp\left\{-2\pi p_D \lambda_R \mathbb{E}_{A_i} \left[\int_r^\infty \left(1 - \frac{1}{1 + s_1 A_i P_R K x^{-\alpha}}\right) x dx\right]\right\} \tag{17} \\
 &\stackrel{(c)}{=} \exp\left\{-2\pi p_D \lambda_R \sum_{k=1}^4 b_k^1 \int_r^\infty \frac{x dx}{1 + (s_1 a_k^1 P_R K)^{-1} x^\alpha}\right\} \\
 &= \prod_{k=1}^4 \exp\left\{-2\pi p_D \lambda_R b_k^1 \int_r^\infty \frac{x dx}{1 + (s_1 a_k^1 P_R K)^{-1} x^\alpha}\right\} \\
 &\stackrel{(d)}{=} \prod_{k=1}^4 \exp\left\{\frac{2\pi p_D \lambda_R \beta_k^1 r^2 b_k^1}{\alpha - 2} {}_2F_1\left(1, 1 - \frac{2}{\alpha}; 2 - \frac{2}{\alpha}; \beta_k^1\right)\right\},
 \end{aligned}$$

where (a) is obtained using the probability generating functional (PGFL) of PPP [12,13]. (b) is obtained using $g_i \sim \exp(1)$. Note that the lower extreme of the integration is r as the distance between the closest interfering RRH in the downlink mode and the typical user is greater than r . This is the distance between the typical user and its serving RRH. (c) is from the probability mass function of A_i . ${}_2F_1(\cdot, \cdot; \cdot; \cdot)$ is the hypergeometric function and $\beta_k^1 = -s_1 a_k^1 P_R K r^{-\alpha}$ [19].

Following similar steps, the expression of $\mathcal{L}_{I_U}(s_1)$ can be obtained in (12).

Finally, substituting (17), (12) and (15) into (14) results in (8). □

Assuming no power control, i.e., $\varepsilon = 0$, (12) can be rewritten as:

$$\mathcal{L}_{I_U}(s) = \prod_{k=1}^3 \exp\left\{\frac{2\pi p_U \lambda_R \beta_k^2 r^2 b_k^2}{\alpha - 2} {}_2F_1\left(1, 1 - \frac{2}{\alpha}; 2 - \frac{2}{\alpha}; \beta_k^2\right)\right\}, \tag{18}$$

where $\beta_k^2 = -s_1 a_k^2 P_U K r^{-\alpha}$ and $\alpha > 2$.

3.2. Uplink SINR Coverage Analysis for Traditional Flexible Duplex

It is assumed that the typical user is at the origin denoted by X and it is associated to the nearest RRH, which is in the uplink mode and is denoted by Z_0 . Therefore, the uplink SINR at the tagged RRH Z_0 can be expressed as:

$$\text{SINR}_{UL} = \frac{P_U M_R M_U h'_{X, Z_0} K^{(1-\varepsilon)} D_{X, Z_0}^{\alpha(\varepsilon-1)}}{N_1 + \tilde{I}_D + \tilde{I}_U}, \tag{19}$$

where N_1 is the noise power at the tagged RRH. h'_{X, Z_0} denotes the channel power gain from the typical user to the tagged RRH, and $h'_{X, Z_0} \sim \exp(1)$. \tilde{I}_D denotes the interference received at the tagged RRH from all RRHs in the downlink mode. This can be defined as:

$$\tilde{I}_D = \sum_{Y_i \in \{\Phi_R^D\}} D_i P_R g'_i K D_{Z_0, Y_i}^{-\alpha}, \tag{20}$$

where g'_i denotes the channel power gain from the i -th interfering downlink RRH, and $g'_i \sim \exp(1)$. D_i denotes the effective antenna gain. \tilde{I}_U denotes the interference received

at the tagged RRH from all of the other uplink users except the typical user, which can be defined as:

$$\tilde{I}_U = \sum_{Z_i \in \Phi_R^U \setminus \{Z_0\}} C_i P_U K^{(1-\epsilon)} D_{Z_i, N(Z_i)}^{\epsilon\alpha} h'_i D_{Z_0, N(Z_i)}^{-\alpha}, \tag{21}$$

where h'_i denotes the channel power gain from the i -th interfering uplink user, and $h'_i \sim \exp(1)$. Z_i denotes the i -th RRH in the uplink mode, and its associated user is $N(Z_i)$. C_i denotes the effective antenna gain.

For convenience and tractability, it is assumed that the distance between the interfering RRH in the downlink mode at Y_i and the tagged RRH at Z_0 can be approximated to the distance between Y_i and the typical user at the origin, i.e.,

$$D_{Z_0, Y_i} = D_{X, Y_i}. \tag{22}$$

Hence, the interference received at the tagged RRH from all of the RRHs in the downlink mode can be approximated to:

$$\bar{I}_D = \sum_{Y_i \in \{\Phi_R^D\}} D_i P_R g'_i K D_{X, Y_i}^{-\alpha}. \tag{23}$$

Similarly, it is assumed that the distance between the interfering uplink user at $N(Z_i)$ and the tagged RRH at Z_0 can be approximated to the distance between the RRH at Z_i and the typical user at the origin:

$$D_{Z_0, N(Z_i)} = D_{X, Z_i}. \tag{24}$$

Section 5 will verify the accuracy of the distance approximation in (22) and (24). Using (24), the interference received at the tagged RRH from all of the other uplink users, except the typical user, can be approximated to:

$$\tilde{I}_U = \sum_{Z_i \in \Phi_R^U \setminus \{Z_0\}} C_i P_U K^{(1-\epsilon)} D_{Z_i, N(Z_i)}^{\epsilon\alpha} h'_i D_{X, Z_i}^{-\alpha}. \tag{25}$$

Theorem 2. For the flexible duplex system, the uplink SINR coverage probability can be computed as:

$$P_{S,UL}(y) = \int_0^\infty e^{-s_2 N_1} \mathcal{L}_{\bar{I}_D}(s_2) \mathcal{L}_{\tilde{I}_U}(s_2) f_D(r) dr, \tag{26}$$

where:

$$s_2 = y(P_U M_R M_U)^{-1} K^{(\epsilon-1)} r^{\alpha(1-\epsilon)}, \tag{27}$$

$$\mathcal{L}_{\bar{I}_D}(s_2) = \prod_{k=1}^3 \exp\left\{ \frac{2\pi p_D \lambda_R \beta_k^3 r^2 b_k^3}{\alpha - 2} {}_2F_1\left(1, 1 - \frac{2}{\alpha}; 2 - \frac{2}{\alpha}; \beta_k^3\right) \right\}, \tag{28}$$

$$\beta_k^3 = -s_2 a_k^3 P_R K r^{-\alpha}, \tag{29}$$

$$\mathcal{L}_{\tilde{I}_U}(s_2) = \prod_{k=1}^4 \exp\left\{ -2\pi p_U \lambda_R b_k^1 \mathbb{E}_{D_{Z_i, N(Z_i)}} \left[\int_r^\infty \frac{xdx}{1 + \left(s_2 a_k^1 P_U K^{(1-\epsilon)} D_{Z_i, N(Z_i)}^{\epsilon\alpha}\right)^{-1} x^\alpha} \right] \right\}, \tag{30}$$

$$f_D(r) = 2\pi \lambda_R r e^{-\pi \lambda_R r^2}. \tag{31}$$

Proof of Theorem 2. By using (2), (19), (23), and (25), the probability of the uplink coverage relative to the SINR threshold y can be written as:

$$\begin{aligned}
 P_{S,UL}(y) &= \mathbb{E}_{D_{X,Z_0}} [\mathbb{P}(\text{SINR}_{UL} > y | D_{X,Z_0})] \\
 &= \int_0^\infty \mathbb{P} \left[\frac{P_U M_R M_U h'_{X,Z_0} K^{(1-\varepsilon)} D_{X,Z_0}^{\alpha(\varepsilon-1)}}{N_1 + \bar{I}_D + \bar{I}_U} > y | D_{X,Z_0} = r \right] f_D(r) dr \\
 &= \int_0^\infty \mathbb{P} \left[h'_{X,Z_0} > y (P_U M_R M_U)^{-1} K^{(\varepsilon-1)} r^{\alpha(1-\varepsilon)} (N_1 + \bar{I}_D + \bar{I}_U) \right] f_D(r) dr,
 \end{aligned} \tag{32}$$

where $f_D(r) = 2\pi\lambda_R r e^{-\pi\lambda_R r^2}$ is similar to the downlink analysis. Let

$$s_2 = y (P_U M_R M_U)^{-1} K^{(\varepsilon-1)} r^{\alpha(1-\varepsilon)},$$

and using the fact that $h'_{X,Z_0} \sim \exp(1)$, the inner probability term in (32) can be further simplified as:

$$\mathbb{P} \left[h'_{X,Z_0} > y (P_U M_R M_U)^{-1} K^{(\varepsilon-1)} r^{\alpha(1-\varepsilon)} (N_1 + \bar{I}_D + \bar{I}_U) \right] = \mathbb{P} \left[h'_{X,Z_0} > s_2 (N_1 + \bar{I}_D + \bar{I}_U) \right] = e^{-s_2 N_1} \mathcal{L}_{\bar{I}_D + \bar{I}_U}(s_2), \tag{33}$$

where $\mathcal{L}_{\bar{I}_D + \bar{I}_U}(\cdot)$ is the Laplace transform of the total interference. Since Φ_R^U and Φ_R^D are independent PPPs, $\mathcal{L}_{\bar{I}_D + \bar{I}_U}(s_2)$ can be rewritten as:

$$\mathcal{L}_{\bar{I}_D + \bar{I}_U}(s_2) = \mathcal{L}_{\bar{I}_D}(s_2) \times \mathcal{L}_{\bar{I}_U}(s_2). \tag{34}$$

First, similar to the calculation of $\mathcal{L}_{\bar{I}_D}(s_1)$ in the proof of Theorem 1, $\mathcal{L}_{\bar{I}_D}(s_2)$ can be calculated as:

$$\begin{aligned}
 \mathcal{L}_{\bar{I}_D}(s_2) &= \mathbb{E} \left[e^{-s_2 \bar{I}_D} \right] = \mathbb{E}_{\Phi_R^D, g'_i, D_i} \left[\exp \left(-s_2 \sum_{Y_i \in \{\Phi_R^D\}} D_i P_R g'_i K D_{X,Y_i}^{-\alpha} \right) \right] \\
 &= \exp \left\{ -2\pi p_D \lambda_R \int_r^\infty \left(1 - \mathbb{E}_{g'_i, D_i} [\exp(-s_2 D_i P_R g'_i K x^{-\alpha})] \right) x dx \right\} \\
 &= \exp \left\{ -2\pi p_D \lambda_R \mathbb{E}_{D_i} \left[\int_r^\infty \left(1 - \frac{1}{1 + s_2 D_i P_R K x^{-\alpha}} \right) x dx \right] \right\} \\
 &= \prod_{k=1}^3 \exp \left\{ -2\pi p_D \lambda_R b_k^3 \int_r^\infty \frac{x dx}{1 + (s_2 a_k^3 P_R K)^{-1} x^\alpha} \right\} \\
 &= \prod_{k=1}^3 \exp \left\{ \frac{2\pi p_D \lambda_R \beta_k^3 r^2 b_k^3}{\alpha - 2} {}_2F_1 \left(1, 1 - \frac{2}{\alpha}; 2 - \frac{2}{\alpha}; \beta_k^3 \right) \right\},
 \end{aligned} \tag{35}$$

where $\beta_k^3 = -s_2 a_k^3 P_R K r^{-\alpha}$.

Following the similar steps, the expression of $\mathcal{L}_{\bar{I}_U}(s_2)$ can be obtained in (30).

Finally, substituting (35), (30) and (33) into (32) results in (26). \square

Assuming no power control, (30) can be rewritten as:

$$\mathcal{L}_{\bar{I}_U}(s_2) = \prod_{k=1}^4 \exp \left\{ \frac{2\pi p_U \lambda_R \beta_k^4 r^2 b_k^1}{\alpha - 2} {}_2F_1 \left(1, 1 - \frac{2}{\alpha}; 2 - \frac{2}{\alpha}; \beta_k^4 \right) \right\}, \tag{36}$$

where $\beta_k^4 = -s_2 a_k^1 P_U K r^{-\alpha}$ and $\alpha > 2$.

3.3. Uplink SINR Coverage Analysis for NAFD

It is assumed that a perfect downlink-to-uplink interference cancellation can be performed for the NAFD system.

Theorem 3. For the NAFD system, the uplink SINR coverage probability can be computed as:

$$P'_{S,UL}(y) = \int_0^{\infty} e^{-s_2 N_1} \mathcal{L}_{\bar{I}_U}(s_2) f_D(r) dr, \quad (37)$$

where the expressions of s_2 , $\mathcal{L}_{\bar{I}_U}$, and $f_D(r)$ are in Theorem 2.

Proof of Theorem 3. The proof can be obtained following similar steps in Theorem 2. \square

4. Rate Analysis

4.1. Instantaneous Rate Analysis

The instantaneous achievable rate (bits/s) can be defined as:

$$\Gamma_{\text{ins}} = W \log_2(1 + \text{SINR}), \quad (38)$$

where W is the bandwidth. The exact rate distribution can be derived using the rate coverage probability $P_R(\gamma) = \mathbb{P}[\Gamma_{\text{ins}} > \gamma]$ [16]. Given the SINR coverage probability, the instantaneous achievable rate coverage probability can be computed as:

$$P_R(\gamma) = \mathbb{P}[W \log_2(1 + \text{SINR}) > \gamma] = \mathbb{P}(\text{SINR} > 2^{\frac{\gamma}{W}} - 1) = P_S(2^{\frac{\gamma}{W}} - 1). \quad (39)$$

4.2. Average Rate Analysis

The average achievable rate (bits/s/Hz) can be defined as:

$$\Gamma_{\text{erg}} = \mathbb{E}[\log_2(1 + \text{SINR})]. \quad (40)$$

Because the expectation of a positive random variable X can be calculated as

$$\mathbb{E}[X] = \int_{u>0} \mathbb{P}(X > u) du,$$

we have

$$\Gamma_{\text{erg}} = \int_0^{\infty} \mathbb{P}[\log_2(1 + \text{SINR}) > u] du. \quad (41)$$

Hence, the average downlink rate and the average uplink rate of the flexible duplex system and the NAFD system are given by:

$$\Gamma_{\text{erg,FD}}^{\text{DL}} = \Gamma_{\text{erg,NAFD}}^{\text{DL}} = \int_0^{\infty} P_{S,DL}(2^u - 1) du, \quad (42)$$

$$\Gamma_{\text{erg,FD}}^{\text{UL}} = \int_0^{\infty} P_{S,UL}(2^u - 1) du, \quad (43)$$

$$\Gamma_{\text{erg,NAFD}}^{\text{UL}} = \int_0^{\infty} P'_{S,UL}(2^u - 1) du. \quad (44)$$

5. Numerical Results and Discussion

5.1. System Parameters

This section first uses the Monte Carlo simulations to verify the accuracy of the analytical results of the SINR coverage probability in Theorems 1 and 2. Subsequently, we compare the uplink SINR coverage probability in the flexible duplex system and the NAFD system. We also compare the overall SINR coverage performance in the flexible duplex system under different RRH antenna parameters. Finally, we discuss the advantage of the rate performance of the NAFD system.

Consider a circular area with radius 500 m, the RRH density is $\lambda_R = 10^{-3}$ RRH/m². Unless otherwise specified, the values of the network parameters are set as follows: bandwidth $W = 400$ MHz, $K = 8.8 \times 10^{-4}$, $\alpha = 3.67$, and $\varepsilon = 0$. The transmission power of

RRHs in the downlink mode and the uplink users are $P_R = 46$ dBm and $P_U = 23$ dBm, respectively. The noise signal power is $N_0 = N_1 = -174$ dBm/Hz. The RRH antenna pattern is $M_R = 7$ dBi, $m_R = 0$ dBi, and $\theta_R = 30^\circ$ while the user antenna pattern is $M_U = 3$ dBi, $m_U = 0$ dBi, and $\theta_U = 30^\circ$.

5.2. Numerical Results

The flexible duplex system has the flexibility to adjust p_D and p_U ($p_D + p_U = 1$) to meet the different demands for the uplink and downlink traffic needs. Figures 3 and 4 validate the accuracy of the derived analytical downlink and uplink SINR coverage probability respectively shown in Theorems 1 and 2. The lines correspond to the theoretical results with the distance approximation. A hollow circle marker and a solid circle marker correspond to the Monte Carlo simulation results with and without the distance approximation, respectively. It is shown that the theoretical results match well with the Monte Carlo simulation results whether the distance approximation is used or not. In addition, as can be seen from Figure 3, a lower p_U achieves a lower downlink SINR coverage probability. With a decrease of p_U , the interference from the uplink user to the target downlink user decreases while the interference from the RRHs in the downlink mode increases. Since the transmission power of the RRHs in the downlink mode is larger than the uplink users, the total interference increases and the coverage probability decreases. Similarly, as shown in Figure 4, a better uplink SINR performance is achieved by increasing p_U .

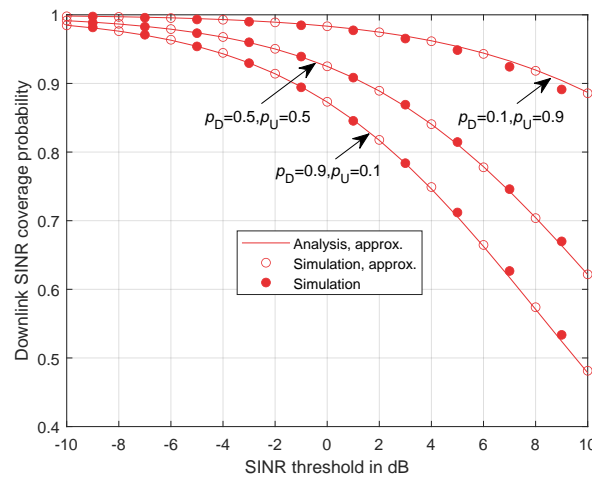


Figure 3. Downlink SINR coverage probability for flexible duplex and NAFD.

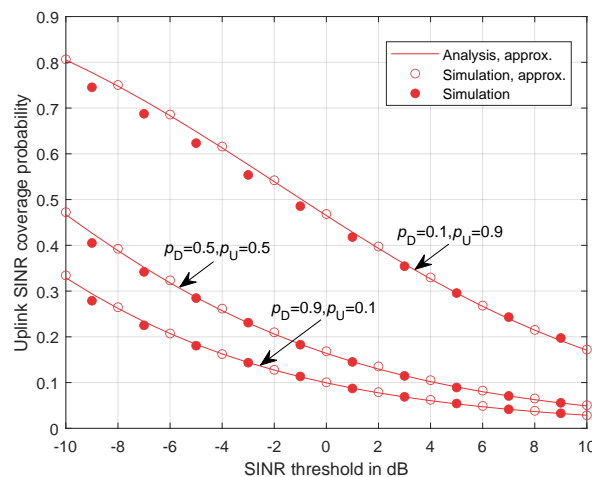


Figure 4. Uplink SINR coverage probability for flexible duplex.

Figure 5 compares the uplink SINR coverage probability in the traditional flexible duplex system and the NAFD system. As demonstrated from Figure 5, the coverage probability of the uplink SINR will increase with the downlink interference cancellation. In addition, the higher the proportion of RRHs in the downlink mode, the greater the increase of the uplink SINR coverage probability. Since there is a larger proportion of RRHs in the downlink mode, more downlink interference will be eliminated; hence, there will be a smaller total interference for the tagged RRH in the uplink mode.

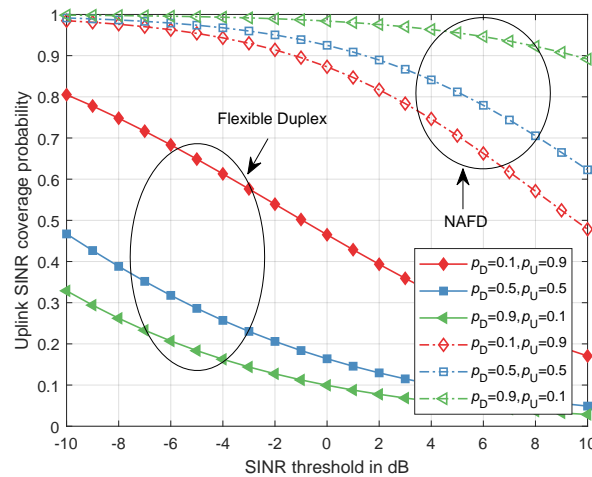


Figure 5. The comparison of uplink SINR coverage probability between the traditional flexible duplex system and the NAFD system.

The total SINR coverage probability for this flexible duplex system can be defined as $P_S(y) = p_D P_{S,DL}(y) + p_U P_{S,UL}(y)$. Figure 6 compares the total SINR coverage probability of the flexible duplex system under different θ_R with $p_D = p_U = 1/2$. Intuitively, when the main lobe gain M_R and the back lobe gain m_R is fixed, a better SINR performance is achieved by decreasing the main lobe beamwidth θ_R .

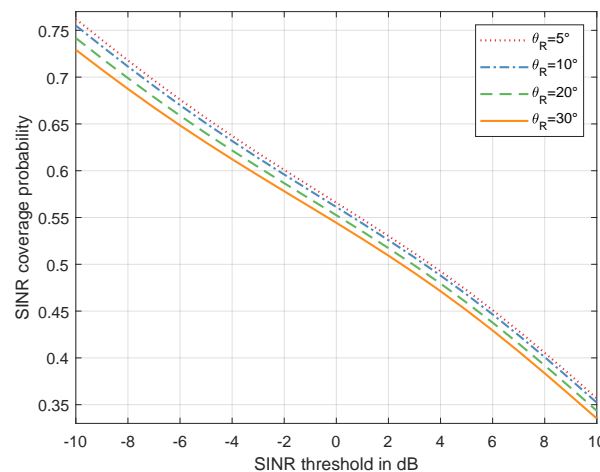


Figure 6. SINR performance with different θ_R .

Figure 7 compares the instantaneous achievable rate coverage probability of the traditional flexible duplex system, the NAFD system and the dynamic TDD system. For the dynamic TDD system, all RRHs perform an uplink transmission or a downlink transmission during a certain time period. Supposing that the time is divided into the frames with a length of T seconds, all RRHs simultaneously receive uplink signals in time period mT and transmit signals in the time interval $(1 - m)T$, where $0 \leq m \leq 1$. To some extent, let

$p_D = p_U = m = 1/2$ to ensure the fairness of the comparison. As illustrated in Figure 7, the NAFD system has a better performance for the instantaneous achievable rate coverage probability than both the flexible duplex system and the dynamic TDD system.

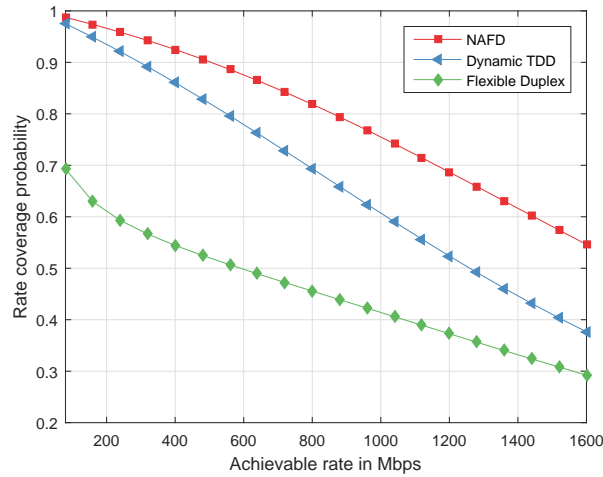


Figure 7. Instantaneous achievable rate performance.

Figure 8 compares the average achievable rate per unit area of the traditional flexible duplex system, the NAFD system, and the dynamic TDD system under different λ_R . Figure 8 shows that with the increase of λ_R , the area spectral efficiency for both systems increase, and the area spectral efficiency of the NAFD system is higher than both the flexible duplex system and the dynamic TDD system.

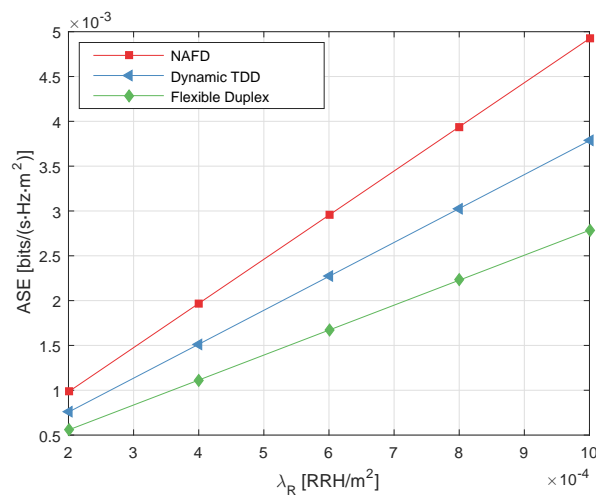


Figure 8. Average achievable rate performance.

5.3. Discussion

From the above numerical results, we have the following remarks. Firstly, the derived analytical downlink and uplink SINR coverage probability respectively shown in Theorems 1 and 2 match well with the Monte Carlo simulation results, which means our theoretical results could be used to demonstrate the system-level performance of mmWave systems with NAFD. Secondly, when all the users use the same frequency bands, the mode selection of RRH is very important for both flexible duplex system and NAFD system. We should optimize the transmitting or receiving mode of each RRH to improve the system-level performance. Thirdly, the numerical results have also demonstrated that when we use large number of antenna elements and reduce beam-width, the probability of cross-link

interference will decrease and the performance of the system will be improved. Finally, we also see that with the ability of cooperative interference cancellation, NAFD has much better performance compared with both the flexible duplex system and the dynamic TDD system.

6. Conclusions

This study analyzed the SINR coverage probability and the spectral efficiency in the flexible duplex system and the NAFD system based on a stochastic geometry framework. We derived the downlink and uplink SINR coverage probability, the instantaneous achievable rate coverage probability, and the average achievable rate. The accuracy of the analytical expressions was verified by Monte Carlo simulations. The numerical results show that the NAFD system outperforms both the flexible duplex system and the dynamic TDD system in spectral efficiency. Since the future communication networks are becoming denser and more heterogeneous, further extensions to our study could include heterogeneous wireless networks.

Author Contributions: Conceptualization, Y.H. and D.W.; writing—original draft preparation, D.Z.; writing—review and editing, Y.H., D.Z., X.X. and D.W.; supervision, Y.H., Z.F., A.L., X.X. and D.W.; project administration, D.W. All authors have read and agreed to the published version of the manuscript.

Funding: This work was supported by the Science and Technology Project of State Grid Corporation of China under Grant SGZJXT00JSJS2000454.

Institutional Review Board Statement: Not applicable.

Informed Consent Statement: Not applicable.

Data Availability Statement: Not applicable.

Acknowledgments: In this section you can acknowledge any support given which is not covered by the author contribution or funding sections. This may include administrative and technical support, or donations in kind (e.g., materials used for experiments).

Conflicts of Interest: The authors declare no conflict of interest.

References

1. Shafi, M.; Molisch, A.F.; Smith, P.J.; Haustein, T.; Zhu, P.; De Silva, P.; Tufvesson, F.; Benjebbour, A.; Wunder, G. 5G: A Tutorial Overview of Standards, Trials, Challenges, Deployment, and Practice. *IEEE J. Sel. Areas Commun.* **2017**, *35*, 1201–1221. [[CrossRef](#)]
2. Zhu, J.; Zhao, M.; Zhou, S. An Optimization Design of Ultra Dense Networks Balancing Mobility and Densification. *IEEE Access* **2018**, *6*, 32339–32348. [[CrossRef](#)]
3. Sun, H.; Wildemeersch, M.; Sheng, M.; Quek, T.Q.S. D2D Enhanced Heterogeneous Cellular Networks With Dynamic TDD. *IEEE Trans. Wirel. Commun.* **2015**, *14*, 4204–4218. [[CrossRef](#)]
4. You, X.; Wang, C.; Huang, J.; Gao, X.; Zhang, Z. Towards 6G wireless communication networks: Vision, enabling technologies, and new paradigm shifts. *Sci. China Inf. Sci.* **2021**, *64*, 110301. [[CrossRef](#)]
5. Agustin, A.; Lagen, S.; Vidal, J.; Munoz, O.; Pascual-Iserte, A.; Guo, Z.; Wen, R. Efficient Use of Paired Spectrum Bands through TDD Small Cell Deployments. *IEEE Commun. Mag.* **2017**, *55*, 210–211. [[CrossRef](#)]
6. Yuan, G.; Zhang, X.; Wang, W.; Yang, Y. Carrier aggregation for LTE-advanced mobile communication systems. *IEEE Commun. Mag.* **2010**, *48*, 88–93. [[CrossRef](#)]
7. Zhong, B.; Chen, L.; Tang, Z. Ergodic rate analysis for full-duplex NOMA networks with energy harvesting. *Sci. China Inf. Sci.* **2021**, *64*, 189303. [[CrossRef](#)]
8. Jeon, W.S.; Jeong, D.G. Comparison of time slot allocation strategies for CDMA/TDD systems. *IEEE J. Sel. Areas Commun.* **2000**, *18*, 1271–1278. [[CrossRef](#)]
9. Nomikos, N.; Trakadas, P.; Hatziefremidis, A.; Voliotis, S. Full-Duplex NOMA Transmission with Single-Antenna Buffer-Aided Relays. *Electronics* **2019**, *8*, 1482. [[CrossRef](#)]
10. Xin, Y.; Yang, L.; Wang, D.; Zhang, R.; You, X. Bidirectional dynamic networks with massive MIMO: Performance analysis. *IET Commun.* **2017**, *11*, 468–476. [[CrossRef](#)]
11. Wang, D.; Wang, M.; Zhu, P.; Li, J.; Wang, J.; You, X. Performance of Network-Assisted Full-Duplex for Cell-Free Massive MIMO. *IEEE Trans. Commun.* **2020**, *68*, 1464–1478. [[CrossRef](#)]
12. Francois Baccelli, B.B. *Stochastic Geometry and Wireless Networks, Part I: Theory*; Now Publishers Inc.: Paris, France, 2009.

13. Chiu, S.N.; Stoyan, D.; Kendall, W.S.; Mecke, J. *Stochastic Geometry and Its Applications*, 3th ed.; Wiley Series in Probability and Statistics; John, Wiley & Sons: Noida, India, 2013.
14. Andrews, J.G.; Gupta, A.K.; Dhillon, H.S. A Primer on Cellular Network Analysis Using Stochastic Geometry. *arXiv* **2016**, arXiv:1604.03183.
15. Andrews, J.G.; Baccelli, F.; Ganti, R.K. A Tractable Approach to Coverage and Rate in Cellular Networks. *IEEE Trans. Commun.* **2011**, *59*, 3122–3134. [[CrossRef](#)]
16. Bai, T.; Heath, R.W. Coverage and Rate Analysis for Millimeter-Wave Cellular Networks. *IEEE Trans. Wirel. Commun.* **2015**, *14*, 1100–1114. [[CrossRef](#)]
17. Singh, S.; Zhang, X.; Andrews, J.G. Joint Rate and SINR Coverage Analysis for Decoupled Uplink-Downlink Biased Cell Associations in HetNets. *IEEE Trans. Wirel. Commun.* **2015**, *14*, 5360–5373. [[CrossRef](#)]
18. Xia, X.; Zhu, P.; Li, J.; Wang, D.; Xin, Y.; You, X. Joint sparse beamforming and power control for large-scale DAS with network assistant full duplex. *IEEE Trans. Veh. Technol.* **2020**, *69*, 7569–7582. [[CrossRef](#)]
19. Gradshteyn, I.; Ryzhik, I. *Table of Integrals, Series, and Products*, 7th ed.; Academic Press: San Diego, CA, USA, 2007.